Article

# Scaling and intermittency in turbulent flows of elastoviscoplastic fluids

**Mohamed S. Abdelgawad** [1,2], **Ianto Cannon** [1,2] & **Marco E. Rosti** [1] ✉

Non-Newtonian fluids have a viscosity that varies with applied stress. Elastoviscoplastic fluids, the elastic, viscous and plastic properties of which are interconnected in a non-trivial way, belong to this category. We have performed numerical simulations to investigate turbulence in elastoviscoplastic fluids at very high Reynolds-number values, as found in landslides and lava flows, focusing on the effect of plasticity. We find that the range of active scales in the energy spectrum reduces when increasing the fluid plasticity; when plastic effects dominate, a new scaling range emerges between the inertial range and the dissipative scales. An extended self-similarity analysis of the structure functions reveals that intermittency is present and grows with the fluid plasticity. The enhanced intermittency is caused by the non-Newtonian dissipation rate, which also exhibits an intermittent behaviour. These findings have relevance to catastrophic events in natural flows, such as landslides and lava flows, where the enhanced intermittency results in stronger extreme events, which are thus more destructive and difficult to predict.

Many fluids in nature and industry exhibit a nonlinear relationship between shear stress and shear rate, which is referred to as non-Newtonian behaviour. Several non-Newtonian features can exist, and they are often present simultaneously. In this Article we focus on the so-called elastoviscoplastic (EVP) fluids, which are fluids with elastic, viscous and plastic properties. EVP materials combine solid-like behaviour and fluid-like response depending on the value of the applied stress: they behave like a solid when the applied stress is below a critical value known as the 'yield stress', and flow like a liquid otherwise[1]. The elastic nature of these materials is present in their solid as well as liquid states[2]. Such fluids are common in everyday life (examples include toothpaste, jam, cosmetics and mud), and turbulent flows of EVP fluids are found in many industrial processes, including sewage treatment, crude oil transportation, concrete pumping and mud drilling[3–5], as well as in nature as landslides and lava flows[6,7].

A great deal of work has been done in the past to properly characterize the viscoelastic behaviour of a fluid in both laminar and turbulent flows[8–13], while the effect of plasticity has been studied mainly in low-Reynolds-number laminar conditions[1,14,15]. Little is known about the plastic behaviour of an EVP fluid in turbulence. Rosti et al.[16] studied

a turbulent channel flow of an EVP fluid, finding that the shape of the mean velocity profile controls the regions where the fluid is unyielded, forming plugs around the channel centreline that grow in size as the yield stress increases, similar to what is observed in a laminar condition. However, the presence of the plug region has an opposite effect on drag for laminar and turbulent flow configurations, resulting in drag reduction in the turbulent case and drag increase in the laminar one; the turbulent drag behaviour is due to the tendency of the turbulent flow to relaminarize, overall leading to a strongly nonlinear relation between yield stress and drag coefficient. Simulation results were then employed by Le Clainche et al.[17], using high-order dynamic mode decomposition, to study the near-wall dynamics, comparing them to those in Newtonian and viscoelastic fluids. Their work revealed that both elasticity and plasticity have similar effects on the near-wall coherent structures, where the flow is characterized by long streaks disturbed for short periods by localized perturbations. A recent experimental study by Mitishita et al.[18] on a turbulent duct flow of Carbopol solution de facto verified the numerical results obtained by Rosti et al.[16] on the effect of plasticity on the mean flow profile and Reynolds stresses. Additionally, they observed an increase in the energy content

[1]Complex Fluids and Flows Unit, Okinawa Institute of Science and Technology Graduate University, Onna-son, Okinawa, Japan. [2]These authors contributed equally: Mohamed S. Abdelgawad, Ianto Cannon. ✉e-mail: marco.rosti@oist.jp
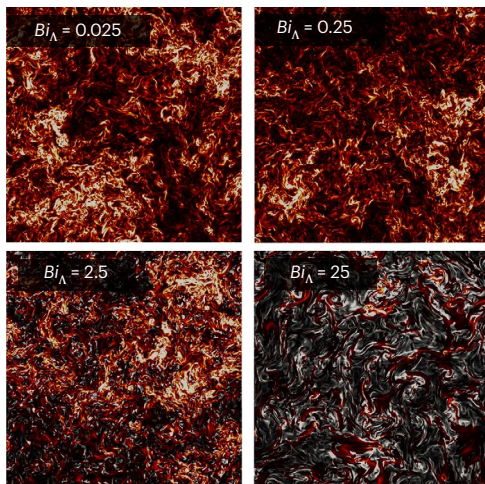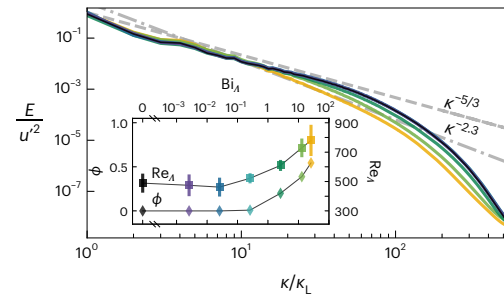
**Fig.1 | Instantaneous colourmaps of the turbulent fluid dissipation $\epsilon_f$ in homogeneous isotropic turbulence of an EVP fluid at different Bingham numbers.** Yielded regions are shown with a black–red–yellow colourscale, and unyielded regions with black–grey–white.



**Fig. 2 | Turbulent kinetic energy spectra of EVP flows with various Bingham numbers.** Different BIngham numbers are plotted in colours from dark to light; $Bi_\Lambda$ = 0, 0.0025, 0.025, 0.25, 2.5, 12.5 and 25 are plotted in black, purple, dark blue, light blue, dark green, light green and orange, respectively. The expected Kolmogorov scaling for a Newtonian fluid is shown by a grey dashed line, and the grey dash-dotted line represents an apparent new non-Newtonian scaling $E \sim \kappa^{-2.3}$ that emerges at large $Bi_\Lambda$. Inset: variation of the mean values of the microscale Reynolds number $Re_\Lambda$ (right axis, plotted as squares) and the volume fraction of the unyielded regions $\Phi$ (left axis, plotted as diamonds) as a function of $Bi_\Lambda$. Error bars report the s.d. of $Re_\Lambda$ in time, measured using $10^3$ samples. Plastic effects start to appear for $Bi_\Lambda \gtrsim 1$, suggesting that $\Lambda$ is the relevant length scale of the problem.

at large scales and a decrease at small scales, when compared with a Newtonian fluid. Mitishita et al. reported a −7/2 scaling in the energy spectra at high wavenumbers during Carbopol flows compared to −5/3 scaling in the case of water flows. The newly observed scaling was attributed either to the decrease in the inertial effect in the presence of Carbopol solutions, which shrinks the inertial range of scales because the Reynolds numbers are much lower than in water flows, or to the elastic effects that become important at large wavenumbers where the fluid experiences high frequencies. Moreover, the shear-thinning effects that Carbopol solutions exhibit affected the anisotropy and the overall flow behaviour. The elastic and shear-thinning effects are rheological features of Carbopol solutions and cannot be eliminated experimentally.

Homogeneous and isotropic turbulent flows have long been a focus of turbulence research for their simple theoretical analysis and the generality of their results. To this end, as has been extensively done in the past for viscoelastic flows, here we study tri-periodic homogeneous flow, where the celebrated K41 theory by Kolmogorov[19] can be directly applied to a classical Newtonian fluid. In this Article we study a homogeneous isotropic turbulent (HIT) flow of an EVP fluid at high Reynolds number, as shown in Fig. 1. We aim to answer the following fundamental question: how does the Kolmogorov theory change when the fluid is EVP? We will mainly focus on its plastic behaviour and investigate how the yield stress affects the multiscale energy distribution and balance, and how the turbulent energy cascade is altered by the fluid's plasticity. Our results show profound modifications of the classical picture predicted by the K41 theory for Newtonian fluids, with the emergence of a new scaling range, the dominance of the non-Newtonian flux and dissipation at small and intermediate scales, and enhanced intermittency of the flow.

## Results

To investigate the problem at hand, we performed massive three-dimensional direct numerical simulations (DNS) of HIT where we solve the flow equations fully coupled with the constitutive equation of the EVP fluid, within a tri-periodic domain of size $L$, using 1,024 grid points per side, as described in more detail in the Methods. The flow is controlled by four main parameters: the Reynolds number $Re_\Lambda$, the Weissenberg number $Wi_\Lambda$, the viscosity ratio $\alpha$ and the Bingham number $Bi_\Lambda$, all based on the root-mean-square velocity fluctuations $u'$ and Taylor's microscale $\Lambda$. We use the definitions

$Re_\Lambda \equiv \rho u' \Lambda / \mu_t$, $Wi_\Lambda \equiv \lambda \mu_t / \rho \Lambda_0^2$, $\alpha = \mu_n / \mu_t$ and $Bi_\Lambda \equiv \tau_y \Lambda_0 / \mu_t u'_0$, where $\rho$ is the fluid density, $\mu_t \equiv \mu_f + \mu_n$ is the total dynamic viscosity with $\mu_f$ being the fluid viscosity and $\mu_n$ the non-Newtonian one, $\lambda$ is the relaxation time, $\tau_y$ is the yield stress, and subscript 0 denotes quantities from the $Bi_\Lambda = 0$ case. The Reynolds number describes the ratio of inertial to viscous forces, and we limit our analysis to high-Reynolds-number flows, achieving a Taylor microscale Reynolds number $Re_\Lambda \approx 435$ for the Newtonian flow, at which statistics of the flow have been found to be universal and exhibiting a proper scale separation, with an extensive inertial range of scales extended to almost two decades of wavenumbers. The Reynolds number explored here is the highest in DNS of HIT of non-Newtonian fluids. The Weissenberg number describes the ratio of elastic to viscous forces, and here we limit the analysis to $Wi_\Lambda \ll 1$ (that is, $Wi_\Lambda \approx 10^{-3}$), to ensure that elastic effects are subdominant and all the observed changes are due to plasticity. We also fix a value of $\alpha = 0.1$ to represent a dilute concentration of polymers, in accordance with previous works on the subject[16,20]. Thus, the key control parameter we vary is $Bi_\Lambda$, which describes the ratio of the yield stress to the viscous stress, and thus correlates with the prevalence of unyielded regions.

Figure 2 depicts the turbulent kinetic energy spectra of the cases analysed. The $Bi_\Lambda = 0$ case is similar to the Newtonian case shown in Supplementary Fig. 1, confirming that the effect of elasticity is subdominant and can be ignored. A clear $E \sim \kappa^{-5/3}$ range is visible for more than one decade, showing that $Re_\Lambda$ is high enough to achieve scale separation, with the spectra exhibiting an inertial range of scales followed by a dissipative range. As $Bi_\Lambda$ increases, the inertial range is limited to the large scales (small wavenumbers $\kappa$), with the energy increasing at large scales and decreasing at small scales. A clear deviation from Kolmogorov scaling becomes noticeable for $Bi_\Lambda > 1$, resulting in the emergence of a new apparent scaling of $E \sim \kappa^{-2.3}$ that is shown more clearly by plotting compensated energy spectra (as shown in Supplementary Fig. 3). The difference in scaling between the experimental work $(-7/2)$[18] and the current study $(-2.3)$ is mainly due to the higher values of Reynolds and Bingham numbers considered here. The abrupt change in the spectra with $Bi_\Lambda$ is consistent with the bulk flow properties ($Re_\Lambda$ and the volume fraction of the unyielded regions $\Phi$) shown in the inset of Fig. 2: for the cases where $Bi_\Lambda < 1$, $Re_\Lambda$ remains relatively unaltered, with $\Phi$ always close to zero, whereas when $Bi_\Lambda$ further increases, the microscale Reynolds number $Re_\Lambda$ and the volume $\Phi$ of the unyielded regions rapidly increase with a similar trend.
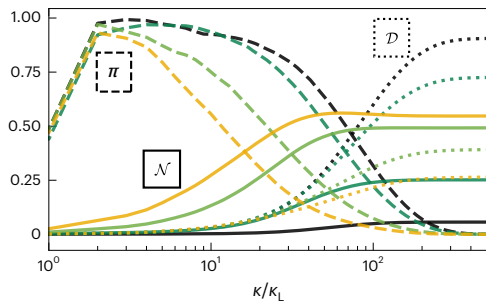
**Fig. 3 | Scale-by-scale energy balance for different $Bi_A$.** Plotted are the energy flux of the nonlinear convective term $\Pi$ (dashed lines), solvent dissipation $\mathcal{D}$ (dotted lines) and the non-Newtonian contribution $\mathcal{N}$ (solid lines) for $Bi_A = 0$ (black), $Bi_A = 2.5$ (dark green), $Bi_A = 12.5$ (light green) and $Bi_A = 25$ (orange). Each term is normalized by the total dissipation rate $\langle \epsilon_t \rangle$. $\mathcal{N}$ grows at intermediate and small scales when $Bi_A$ is increased, eventually becoming the dominant contribution.

To fully characterize the change in the energy spectra, we study the turbulent kinetic energy balance, which in wavenumber space can be expressed as

$$\mathcal{F}_{inj}(\kappa) + \Pi(\kappa) + \mathcal{D}(\kappa) + \mathcal{N}(\kappa) = \langle \epsilon_f \rangle + \langle \epsilon_n \rangle = \langle \epsilon_t \rangle, \quad (1)$$

where $\mathcal{F}_{inj}$ is the turbulence production introduced by the external forcing (injected at the largest scale, $\kappa_L \equiv 2\pi/L$), and $\Pi$, $\mathcal{D}$ and $\mathcal{N}$ are the nonlinear energy flux, the fluid dissipation and the non-Newtonian contribution, respectively. In addition to the classical bulk fluid dissipation rate $\epsilon_f$, here we have a non-Newtonian dissipation $\epsilon_n$, which is the rate of removal of turbulent kinetic energy from the flow due to the non-Newtonian extra stress tensor (Supplementary Sections I and II provide a derivation of this equation). Figure 3 shows the turbulent kinetic energy balance for a few representative values of $Bi_A$. When comparing with Supplementary Fig. 1b, the $Bi_A = 0$ case closely follows the classical Newtonian turbulent flow, where energy is carried by $\Pi$ from the large to small scales before being dissipated by the fluid viscosity $\mathcal{D}$. The contribution of the nonlinear convective term $\Pi$, which appears as an almost horizontal plateau at relatively large scales, progressively decreases with $Bi_A$ and shrinks towards larger scales, consistent with the reduction of the extension of the inertial range observed in Fig. 2. The reduced energy flux with $Bi_A$ is also accompanied by a decrease of the fluid dissipation $\mathcal{D}$, which is instead compensated by the increase of non-Newtonian contribution $\mathcal{N}$. At small scales (large $\kappa$), the relative importance of the non-Newtonian contribution increases with $Bi_A$, becoming comparable to the fluid dissipation for $Bi_A \approx 2.5$ and eventually becoming the dominant term for $Bi_A \gtrsim 12.5$, corresponding to the emergence of the new scaling in the energy spectrum shown in Fig. 2; indeed, the non-Newtonian contribution can be interpreted as a combination of a pure energy flux (giving rise to the new scaling region) and a pure dissipative term, as recently suggested by Rosti and others[21]. Regarding the direction of energy flux, Supplementary Fig. 4 shows that we have a direct cascade of energy from large to small scales for all $Bi_A$ (refs. [22,23]).

We extend the analysis done in the spectral domain by computing the longitudinal structure functions defined as $S_p(r) = \langle (\Delta u(r))^p \rangle$, where $p$ is the order of the structure function and $\Delta u(r) = u(x + r) - u(x)$ is the difference in the fluid velocity across a length scale $r$, projected in the direction of $r$. According to K41, $S_p(r) \sim \langle \epsilon_t \rangle r \rangle^{p/3}$; however, when the structure functions are displayed as a function of $r$, as shown in Fig. 4a, they deviate from the K41 prediction as $p$ increases. This phenomenon is thought to be due to the intermittency of the flow, that is, extreme events that are localized in space and time, and thereby break Kolmogorov's hypothesis of self-similarity in the inertial range[24].

Intermittency results in the scaling exponent of $r$ being a nonlinear concave function of $p$ (instead of $p/3$)[25]. For the EVP fluid, two scaling regions appear at large $Bi_A$, with scaling consistent with those from the energy spectra, and with intermittency present in both scaling regions. The role of intermittency in the scaling exponents can be better appreciated when the structure functions are displayed in their extended self-similarity form, obtained by plotting one structure function against another[26]. In Fig. 4b, $S_4$ and $S_6$ are plotted against $S_2$ for all Bingham numbers considered. We note a clear power-law scaling, which deviates from Kolmogorov's prediction, even for the $Bi_A = 0$ case (shown in black). The departure from Kolmogorov's prediction progressively grows as the plasticity of the fluid increases, suggesting that the flow becomes more intermittent due to its plasticity. This becomes more obvious when we plot $S_n$ compensated by the intermittency correction at $Bi_A = 0$ against $S_2$ (Supplementary Fig. 5). Also, intermittency appears to act equally in the two scaling regions present at large $Bi_A$.

Intermittency originates from the multifractal nature of the turbulent dissipation rate[24]. For Newtonian fluids, this can be quantified by the multifractal spectrum of the energy dissipation rate, $\epsilon_f$ (refs. [24,27]), which we report in the inset of Fig. 4b. This graph demonstrates that $F(\alpha)$ is nearly identical for all $Bi_A$ cases except for minor variations at small and large values of $\alpha$. This implies that the fluid dissipation rate is not the cause of the enhanced intermittency observed in the extended self-similarity analysis.

In the present flow, the turbulent kinetic energy is dissipated by two different terms, $\epsilon_f$ and $\epsilon_n$, as seen in Fig. 1. We thus investigate their respective behaviour by looking at their probability distribution functions (PDFs; Fig. 5). We name the non-Newtonian contribution $\epsilon_n$ a 'dissipation' because, on average, it removes energy from the flow, giving rise to the positive-skewed distributions in Fig. 5b; however, unlike the fluid dissipation, it can take positive or negative values at particular locations in space and time. Figure 5a shows that the distribution of $\epsilon_f$ narrows as $Bi_A$ increases[28]; on the other hand, from Fig. 5b, we see that that the distribution of $\epsilon_n$ substantially broadens as $Bi_A$ increases. Because the non-Newtonian dissipation becomes dominant for the largest $Bi_A$ (as shown in Fig. 3), we can thus infer that the extreme values of $\epsilon_n$ are indeed the source of the enhanced intermittency observed from the structure function analysis in Fig. 4.

## Discussion

By means of unprecedented high-Reynolds-number DNS of an EVP fluid, we have shown that plastic effects substantially alter the classical turbulence predicted by Kolmogorov theory for Newtonian fluids.

We have proved that the non-Newtonian contribution to the energy balance becomes dominant at intermediate and small scales for large Bingham numbers, inducing the emergence of a new intermediate scaling range in the energy spectra between the Kolmogorov inertial and dissipative ranges, where the energy spectrum decays with a $-2.3$ exponent. Interestingly, this exponent has been recently found for the turbulence of viscoelastic fluids at large Reynolds and Weissenberg numbers[21,29], suggesting a possible similarity among plastic and elastic effects on the turbulent cascade. This similarity in the scaling behaviour of the two cases could be attributed to a similar interaction mechanism in the Navier–Stokes equation between the convective and extra stress terms. It is also worth noting that in the context of viscoelastic flows at high Weissenberg number, an exponent less than or equal to $-3$ has been widely reported in the past[8]; however, this is only found at relatively lower Reynolds number than investigated here or explored in recent experimental and numerical work[21,29]. The present work reports the $-2.3$ scaling in turbulent flows of highly plastic EVP fluids, and further studies on the size and distribution of the unyielded regions could shed more light on the origin of the newly found scaling.

We have also shown that the flow in the presence of plastic effects is more intermittent than in a Newtonian fluid, due to the combination of the classical intermittency originating from the multifractal
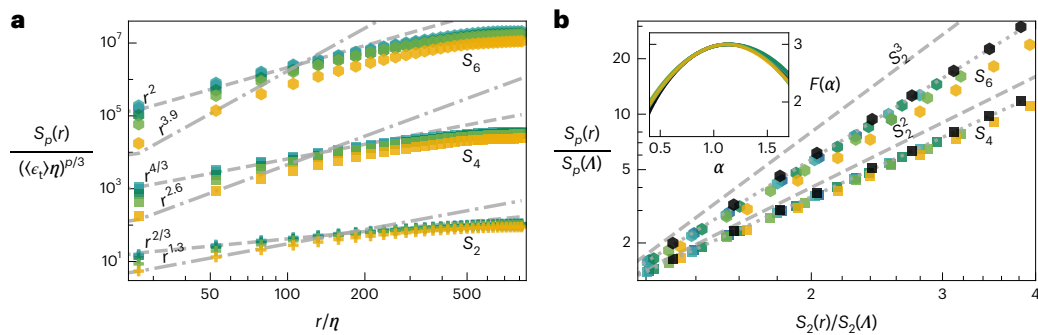
**Fig. 4 | Analysis of structure functions. a**, Dependence of the longitudinal velocity structure functions $S_2$ (pluses), $S_4$ (squares) and $S_6$ (hexagons) on separation distance $r$. Symbol colour denotes $Bi_A$ and is the same as in Fig. 2. Dashed lines show scalings predicted by K41, and dash-dotted lines show scalings predicted using the new non-Newtonian scaling $E \sim \kappa^{-2.3}$. **b**, The two scalings collapse onto a single line when we plot the structure functions $S_4$ and $S_6$ in extended self-similarity form, that is, against $S_2$. To easily see changes in gradient, we have normalized the structure functions by their values at $r \approx \Lambda$. The dotted line shows a best fit through the data for $Bi_A = 0$, which deviates from the K41 prediction (dashed line) due to intermittency. Increasing $Bi_A$ further increases this deviation. The inset in **b** reports the multifractal spectrum of the energy dissipation rate carried out by the fluid $\epsilon_f$.
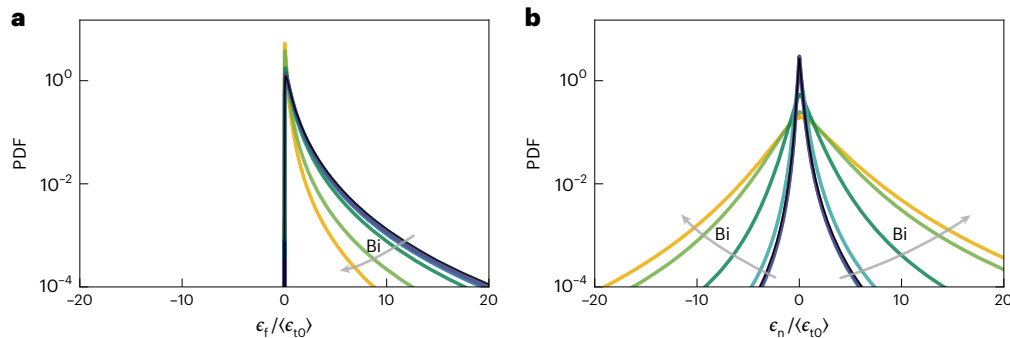


**Fig. 5 | PDFs of the fluid dissipation rate $\epsilon_f$ and non-Newtonian dissipation rate $\epsilon_n$. a,b**, PDF of the fluid dissipation rate $\epsilon_f$ (**a**) and of the non-Newtonian dissipation rate $\epsilon_n$ (**b**) averaged over time, and normalized by $\langle \epsilon_0 \rangle$, the total dissipation of the $Bi_A = 0$ flow. As $Bi_A$ increases, the PDF of $\epsilon_f$ narrows slightly, whereas the PDF of $\epsilon_n$ widens substantially.

nature of the turbulent dissipation rate, which remains substantially unaltered, and a new plastic contribution that instead grows with the Bingham number. A direct consequence of this result is that intermittency corrections for an EVP fluid are non-universal and dependent on the flow configuration, differently from viscoelastic flows. These results are relevant for several catastrophic natural flows with high plasticity, such as lava flows and landslides[30]. Our findings explain why such flows are usually found to be intermittent and frequently aggressive, resulting in more damage. The non-universality of the flow intermittency in EVP fluids reflects also in an increased difficulty in their modelling.

## Online content

Any methods, additional references, Nature Portfolio reporting summaries, source data, extended data, supplementary information, acknowledgements, peer review information; details of author contributions and competing interests; and statements of data and code availability are available at https://doi.org/10.1038/s41567-023-02018-2.

## References

1. Balmforth, N. J., Frigaard, I. A. & Ovarlez, G. Yielding to stress: recent developments in viscoplastic fluid mechanics. *Annu. Rev. Fluid Mech.* **46**, 121–146 (2014).
2. Fraggedakis, D., Dimakopoulos, Y. & Tsamopoulos, J. Yielding the yield-stress analysis: a study focused on the effects of elasticity on the settling of a single spherical particle in simple yield-stress fluids. *Soft Matter* **12**, 5378–5401 (2016).
3. Hanks, R. W. The laminar-turbulent transition for flow in pipes, concentric annuli and parallel plates. *Aiche J.* **9**, 45–48 (1963).
4. Hanks, R. W. On the flow of Bingham plastic slurries in pipes and between parallel plates. *Soc. Petrol. Eng. J.* **7**, 342–346 (1967).
5. Maleki, A. & Hormozi, S. Submerged jet shearing of visco-plastic sludge. *J. Non-Newtonian Fluid Mech.* **252**, 19–27 (2018).
6. Jerolmack, D. J. & Daniels, K. E. Viewing Earth's surface as a soft-matter landscape. *Nat. Rev. Phys.* **1**, 716–730 (2019).
7. Jones, T. J., Reynolds, C. D. & Boothroyd, S. C. Fluid dynamic induced break-up during volcanic eruptions. *Nat. Commun.* **10**, 3828 (2019).
8. Groisman, A. & Steinberg, V. Elastic turbulence in a polymer solution flow. *Nature* **405**, 53–55 (2000).
9. Poole, R. J., Alves, M. A. & Oliveira, P. J. Purely elastic flow asymmetries. *Phys. Rev. Lett.* **99**, 164503 (2007).
10. Haward, S. J., Mckinley, G. H. & Shen, A. Q. Elastic instabilities in planar elongational flow of monodisperse polymer solutions. *Sci. Rep.* **6**, 33029 (2016).
11. Steinberg, V. Elastic turbulence: an experimental view on inertialess random flow. *Annu. Rev. Fluid Mech.* **53**, 27–58 (2021).
12. Datta, S. S. et al. Perspectives on viscoelastic flow instabilities and elastic turbulence. *Phys. Rev. Fluids* **7**, 080701 (2022).
13. Abreu, H., Pinho, F. T. & da Silva, C. B. Turbulent entrainment in viscoelastic fluids. *J. Fluid Mech.* **934**, A36 (2022).

14. Pavlov, K. B., Romanov, A. S. & Simkhovich, S. L. Hydrodynamic stability of poiseuille flow of a viscoplastic non-Newtonian fluid. *Fluid Dynamics* **9**, 996–998 (1974).

15. Escudier, M. P. et al. Observations of asymmetrical flow behaviour in transitional pipe flow of yield-stress and other shear-thinning liquids. *J. Non-Newtonian Fluid Mech.* **127**, 143–155 (2005).

16. Rosti, M. E., Izbassarov, D., Tammisola, O., Hormozi, S. & Brandt, L. Turbulent channel flow of an elastoviscoplastic fluid. *J. Fluid Mech.* **853**, 488–514 (2018).

17. Le Clainche, S., Izbassarov, D., Rosti, M., Brandt, L. & Tammisola, O. Coherent structures in the turbulent channel flow of an elastoviscoplastic fluid. *J. Fluid Mech.* **888**, A5 (2020).

18. Mitishita, R. S., MacKenzie, J. A., Elfring, G. J. & Frigaard, I. A. Fully turbulent flows of viscoplastic fluids in a rectangular duct. *J. Non-Newtonian Fluid Mech.* **293**, 104570 (2021).

19. Kolmogorov, A. The local structure of turbulence in incompressible viscous fluid for very large Reynolds' numbers. *Akademiia Nauk SSSR Doklady* **30**, 301–305 (1941).

20. Perlekar, P., Mitra, D. & Pandit, R. Manifestations of drag reduction by polymer additives in decaying, homogeneous, isotropic turbulence. *Phys. Rev. Lett.* **97**, 3–6 (2006).

21. Rosti, M. E., Perlekar, P. & Mitra, D. Large is different: non-monotonic behaviour of elastic range scaling in polymeric turbulence at large Reynolds and Deborah numbers. *Sci. Adv.* **9**, eadd3831 (2023).

22. Xia, H., Byrne, D., Falkovich, G. & Shats, M. Upscale energy transfer in thick turbulent fluid layers. *Nat. Phys.* **7**, 321–324 (2011).

23. Cerbus, R. T. & Chakraborty, P. The third-order structure function in two dimensions: the Rashomon effect. *Phys. Fluids* **29**, 111110 (2017).

24. Frisch, U. *Turbulence: The Legacy of A. N. Kolmogorov* (Cambridge Univ. Press, 1995).

25. Kolmogorov, A. N. A refinement of previous hypotheses concerning the local structure of turbulence in a viscous incompressible fluid at high Reynolds number. *J. Fluid Mech.* **13**, 82–85 (1962).

26. Benzi, R. et al. Extended self-similarity in turbulent flows. *Phys. Rev. E* **48**, R29–R32 (1993).

27. Mandelbrot, B. B. Intermittent turbulence in self-similar cascades: divergence of high moments and dimension of the carrier. *J. Fluid Mech.* **62**, 331–358 (1974).

28. Donzis, D. A., Sreenivasan, K. R. & Yeung, P. K. Scalar dissipation rate and dissipative anomaly in isotropic turbulence. *J. Fluid Mech.* **532**, 199–216 (2005).

29. Zhang, Y. B., Bodenschatz, E., Xu, H. & Xi, H. D. Experimental observation of the elastic range scaling in turbulent flow with polymer additives. *Sci. Adv.* **7**, eabd3525 (2021).

30. Schaeffer, D. G. & Iverson, R. M. Steady and intermittent slipping in a model of landslide motion regulated by pore-pressure feedback. *SIAM J. Appl. Math.* **69**, 769–786 (2008).

## Methods

### Governing equations

The flow under investigation is governed by a system of a scalar, a vector and a tensorial equation—the incompressibility constraint, the conservation of momentum, and the constitutive equation for the non-Newtonian extra stress tensor, respectively. The incompressibility constraint and the momentum conservation equations can be written as

$$\nabla \cdot \mathbf{u} = 0, \tag{2}$$

$$\rho\left(\frac{\partial \mathbf{u}}{\partial t} + \mathbf{u} \cdot \nabla \mathbf{u}\right) = \nabla p + \mu_f \nabla^2 \mathbf{u} + \mathbf{f}_{inj} + \mathbf{f}_{evp}, \tag{3}$$

where $\mathbf{u}$ is the fluid velocity, $p$ is the pressure, $\rho$ is the density and $\mu_f$ is the fluid dynamic viscosity. The term $\mathbf{f}_{inj}$ represents the external force used to sustain turbulence; here we consider the Arnold–Beltrami–Childress (ABC) flow with forcing

$$
\begin{aligned}
\mathbf{f}_{inj} = &\,\mathbf{i}\mu_f(A\sin z/L + C\cos y/L) + \mathbf{j}\mu_f(B\sin y/L + A\cos z/L) \\
&+ \mathbf{k}\mu_f(C\sin y/L + B\cos x/L),
\end{aligned} \tag{4}
$$

where $\mathbf{i}$, $\mathbf{j}$ and $\mathbf{k}$ are the Cartesian unit vectors, $A$, $B$ and $C$ are real parameters, and the flow has periodicity $L$ in $x$, $y$ and $z$. In our simulations, we choose $A = B = C$ and use an appropriate value of $\mu_f$ to give a microscale Reynolds number $\mathrm{Re}_\Lambda \approx 435$ for the Newtonian flow. The last term in equation (3) is defined as $\mathbf{f}_{evp} \equiv \nabla \cdot \boldsymbol{\tau}$, where $\boldsymbol{\tau}$ is the non-Newtonian extra stress tensor of the EVP fluid. We adopt the constitutive model proposed by Saramito[31] to express the evolution of the extra stress tensor, which can be written as

$$\lambda \stackrel{\triangledown}{\boldsymbol{\tau}} + \max\left(0, \frac{\tau_d - \tau_y}{\tau_d}\right)\boldsymbol{\tau} = \mu_n\left(\nabla \mathbf{u} + (\nabla \mathbf{u})^T\right) \tag{5}$$

where $(\stackrel{\triangledown}{\cdot})$ denotes the upper convected derivative, that is, $\stackrel{\triangledown}{\boldsymbol{\tau}} = \frac{\partial \boldsymbol{\tau}}{\partial t} + \mathbf{u} \cdot \nabla \boldsymbol{\tau} - \boldsymbol{\tau} \cdot \nabla \mathbf{u} - (\nabla \mathbf{u})^T \cdot \boldsymbol{\tau}$. $\mu_n$ is the non-Newtonian dynamic viscosity, $\tau_d$ is the magnitude of the deviatoric part of the stress tensor $\boldsymbol{\tau}_d \equiv \boldsymbol{\tau} - \mathrm{tr}(\boldsymbol{\tau})\mathbf{I}/3$, and $\mathbf{I}$ is the identity tensor, that is, $\tau_d = \sqrt{\frac{1}{2}(\boldsymbol{\tau}_d : \boldsymbol{\tau}_d)}$. Before yielding, that is, $\tau_d \le \tau_y$, the model predicts only recoverable Kelvin–Voigt viscoelastic deformation; after yielding, that is, $\tau_d > \tau_y$, it predicts Oldroyd-B viscoelastic behaviour. This transition occurs in a continuous manner. There are other EVP models that take into account shear-thinning[32] or thixotropic behaviour[33]; however, we chose the one described above for its simplicity and the least number of involved parameters. Also, this model proved able to capture the main flow characteristics in a turbulent channel flow[16,18].

### Numerical method

We use the in-house flow solver Fujin (https://groups.oist.jp/cffu/code) to solve the governing equations numerically on a staggered uniform Cartesian grid. Velocities are located on the cell faces, and pressure, stresses and the other material properties are located at the cell centres. The second-order central finite-difference scheme is used for spatial discretization except for the advection term that comes from the upper convective derivative in equation (5), where the fifth-order WENO (weighted essentially non-oscillatory) scheme is adopted[34]. The second-order Adams–Bashforth scheme coupled with a fractional step method[35] is used for the time advancement of all terms except for the non-Newtonian extra stress tensor, which is advanced with the Crank–Nicolson scheme. To enforce a divergence-free velocity field, a fast Poisson solver based on the fast Fourier transform is used for the pressure. The domain decomposition library 2decomp (http://www.2decomp.org) and the MPI protocol are used to parallelize the solver. The evolution equation of the extra EVP stress is formulated and solved using the log-conformation method[36] to ensure the positive-definiteness of the conformation tensor. The fluid domain is a periodic cubic box of length $L$ discretized using 1,024 grid points per side, resulting in a large grid resolution sufficient to represent the fluid properties at all the scales of interest with $\eta/\Delta x = \mathcal{O}(1)$, where $\eta$ is the Kolmogorov length-scale, and $\Delta x$ is the grid spacing.

## References

31. Saramito, P. A new constitutive equation for elastoviscoplastic fluid flows. *J. Non-Newtonian Fluid Mech.* **145**, 1–14 (2007).
32. Saramito, P. A new elastoviscoplastic model based on the Herschel-Bulkley viscoplastic model. *J. Non-Newtonian Fluid Mech.* **158**, 154–161 (2009).
33. Dimitriou, C. J. & McKinley, G. H. A canonical framework for modeling elasto-viscoplasticity in complex fluids. *J. Non-Newtonian Fluid Mech.* **265**, 116–132 (2019).
34. Shu, C. W. High order weighted essentially nonoscillatory schemes for convection dominated problems. *SIAM Rev.* **51**, 82–126 (2009).
35. Kim, J. & Moin, P. Application of a fractional-step method to incompressible Navier-Stokes equations. *J. Comput. Phys.* **59**, 308–323 (1985).
36. Izbassarov, D. et al. Computational modeling of multiphase viscoelastic and elastoviscoplastic flows. *Int. J. Numer. Methods Fluids* **88**, 521–543 (2018).

## Author contributions

M.E.R. conceived the original idea, planned the research and developed the code. All authors performed the numerical simulations, analysed data, outlined the manuscript content and wrote the manuscript.

## Competing interests

The authors declare no competing interests.

## Additional information

**Supplementary information** The online version contains supplementary material available at https://doi.org/10.1038/s41567-023-02018-2.

**Correspondence and requests for materials** should be addressed to Marco E. Rosti.

**Peer review information** *Nature Physics* thanks Cherif Nouar and the other, anonymous, reviewer(s) for their contribution to the peer review of this work.

**Reprints and permissions information** is available at www.nature.com/reprints.